Evolution of Porosity and Channelization of an Erosive Medium Driven by Fluid Flow

Arshad Kudrolli[*] and Xavier Clotet

Department of Physics, Clark University, Worcester, Massachusetts 01610, USA
(Received 30 December 2015; published 7 July 2016)

We demonstrate that a homogeneous porous medium composed of sedimentary particles develops channels due to curvature driven growth of fluid flow coupled with an increase in porosity. While the flux is increased linearly, the evolution of porosity is observed to be intermittent with erosion occurring at the boundaries between low and high porosity regions. Calculating the spatial distribution of the flow within the medium and the fluid stress given by the product of the fluid flux and the volume fraction of the particles, we find that the system organizes itself to be locally near the threshold needed to erode the weakest particles. A statistical model simulating the coupling of the erosion, transport, and deposition of the particles to the local fluid flow and porosity is found to capture the overall development of the observed channels.

Change in porosity of an erodible medium induced by fluid flow is important to the structure of aquifers, dam breaks, and many aspects of extraction and sequestration of hydrocarbons in the subsurface [1–7]. High rates of fluid injection in hydraulic fracturing have been shown to be correlated with higher incidences of seismicity [8]. Porosity changes can occur due to several reasons ranging from hydrodynamic interactions with the flow to reactive transport that dissolves away material resulting in ramified patterns, caves and wormholes in initially homogeneous porous rock [1,9,10], and growth of active matter [11]. Here, we focus on hydrodynamic processes which lead to heterogeneity of a granular bed as a step toward understanding this broad range of problems.

Significant work examining erosion and network growth at the surface of an erodible bed due to runoffs and seepage flow has been reported [12–15]. While these studies provide valuable perspective, the overland flow dynamics can be rather different from those within the subsurface. Studies of fluid injected into loosely consolidated granular materials have been performed motivated by finding analogies to Saffman-Taylor instability in zero-surface tension fluids [16–18] and capillary fracturing [19,20]. Further, the effect of the flow on the conversion of the solid phase to eroded material due to the hydrodynamic shear stress and the frictional stress of the mobile particles carried by the liquid and its feedback on the growth of heterogeneity and channel networks have been considered only recently [21]. However, most experimental studies investigating the changes in porosity due to erosion have been limited to measurement of overall throughput [22,23] because of the difficulties in obtaining dynamic properties within the bulk.

We investigate the spatial evolution of porosity when a fluid is pumped through an erodible medium due to internal erosion by developing a quasi-two-dimensional model of

particles contained within a thin fracture. The experimental system consists of a horizontal rectangular glass chamber which is $L = 290$ mm long, $W = 292$ mm wide, and $h = 1.85$ mm high [see Fig. 1(a)]. The medium is prepared by tilting the system slightly and slowly depositing glass particles with diameter $d = 1.21 \pm 0.1$ mm and density 2500 kg m^{-3} down the incline into the chamber. A narrow ledge separates the chamber and the inlet reservoir preventing the particles from moving into the inlet reservoir. The deposited particles quickly come to rest after colliding with the particles which are already present. This fact is exploited to shape the initial interface by varying the amount of particles poured as a function of width and obtain a monolayer with a volume fraction of particles $\phi = 0.43 \pm 0.02$ [24]. Water with density $\rho_f = 1000$ kg m^{-3} and viscosity $\nu = 0.89$ mPa s is injected uniformly across the system with a prescribed flux J_f. In order to further initialize the system, water is injected with $J_f = 0.15$ mm s^{-1} to fully immerse the chamber in water and prevent any air pockets from forming. Then, the system is kept horizontal, and the flow rate is ramped to a desired value to begin an experimental run. A reservoir at the exit
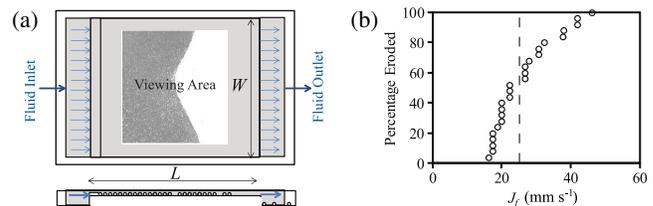
FIG. 1. (a) A schematic top and side view of the experimental apparatus. (b) The percentage of isolated grains observed to move as a function fluid flux J_f. The vertical dashed line corresponds to the mean fluid flux $J_c = 26.3$ mm s^{-1} required to dislodge a grain at rest on the substrate.
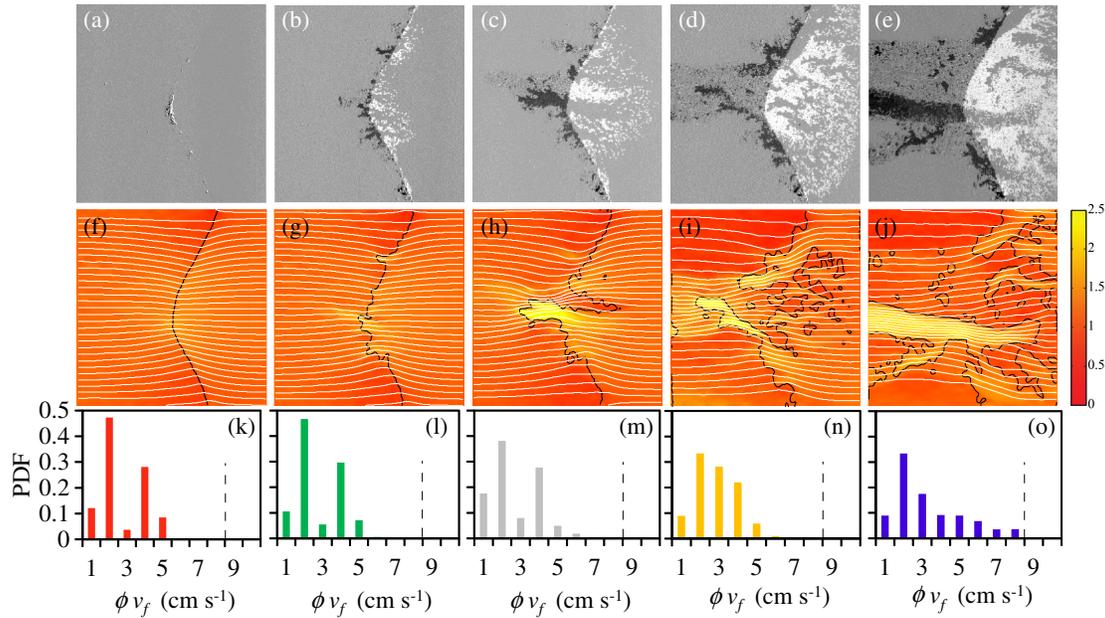
FIG. 2. (a)–(e) Difference images of the central $207d \times 215d$ area of the system indicate where erosion (black) and deposition (white) have occurred as the flow is increased. (a) $J_f/J_c = 0.06$, (b) $J_f/J_c = 0.41$, (c) $J_f/J_c = 0.52$, (d) $J_f/J_c = 0.54$, and (e) $J_f/J_c = 0.64$. (f)–(j) v_f normalized by the corresponding J_f and the streamlines (white line) are plotted in the row below. A contour corresponding to $\phi = 0.22$ (black line) demarcates regions with high and low porosity. (k)–(o) Probability distribution functions (PDFs) of the product of ϕ and v_f. All values are to the left of the vertical dashed line (see text).

collects any eroded material which leaves the chamber and, thus, prevents it from recirculating. The system is illuminated using a collimated beam of light which passes straight through the liquid but bends when passing through the glass particles rendering them dark. This contrast is used to track the particles and obtain ϕ.

To measure the flux required to dislodge particles at rest on the substrate, experiments were performed with particles dispersed sparsely inside the chamber. From the percentage of particles that are dislodged as a function of J_f [see Fig. 1(b)], we find the mean critical flux $J_c = 26.3 \, \text{mm s}^{-1}$ and the standard deviation $\sigma_c = 8.9 \, \text{mm s}^{-1}$. The dispersion arises due to the size distribution and nonsphericity of the particles. While smaller particles are easier to dislodge compared to large ones [25], a particle can have a different threshold for motion depending on its projected surface area perpendicular to the flow and its center of mass relative to the pivot point on the substrate depending on its nonsphericity and roughness. This can lead even a single particle to have a distribution of thresholds for motion depending on its sphericity. Nonetheless, the mean fluid flux J_c can be used as a reference to understand the conditions required to erode particles in the porous medium.

We first discuss the evolution of porosity starting with an example where the medium is prepared with a concave interface between low and high porosity regions. Figures 2(a)–2(e) show difference images of the medium as the fluid flux is increased linearly. We observe that particles erode initially

near the interface with the greatest concavity but travel only a short distance before getting redeposited. If the flow rate is now held constant at this point, no further erosion is observed. As the flux is increased, erosion spreads to a wider region, and the eroded particles move further before redepositing, leading to a roughening of the interface. A channel develops and grows upstream with time, while the redeposited particles spread out in the shape of a river delta with secondary channels. In contrast with studies in which air is injected into a fluid-particle mixture and where surface tension is important [26], the interface appears more diffused, and no significant piling of grains at the interface can be observed in our experiments. Thus, the observed growth is more similar to curvature driven growth of seepage channels observed in granular beds [27] and river delta formation [28] than the invasion of a front as in Saffman-Taylor instability [22,23].

To quantify the dynamics of erosion, we plot the volume fraction of the particles which are mobile ϕ_m as J_f is increased in Fig. 3(a). Here, particles are defined as mobile if they move a distance of at least $d/5$ in 1 s. Small precursors are observed (see magnified plot in the inset) before a large avalanche occurs when $J_f/J_c \sim 0.34$. Even after this event, the erosion is not continuous in time but rather progresses in avalanches, as also observed near channel heads in seepage driven erosion [27]. To elucidate the packing dynamics, we plot in Fig. 3(b) the change in volume fraction $\Delta\phi_{\text{ave}}$ averaged over the viewing area. Slip-stick motion is observed similar to other driven systems such as grains partially filled in a rotated drum
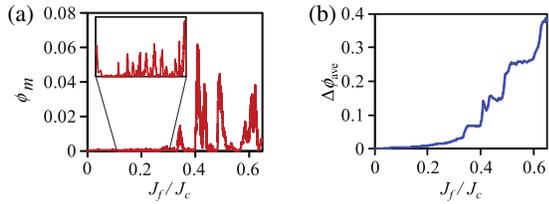
FIG. 3. (a) ϕ_m as a function of increasing imposed flux. Inset: Precursors can be observed before the large avalanche at $J_f/J_c \sim 0.34$. (b) $\Delta\phi_{\mathrm{ave}}$ as a function of J_f shows slip-stick motion.

[29]. This collective behavior can be understood from the fact that the erosion of a particle in the packing is not only dependent on the stress applied by the fluid but also on the net force applied by the particles in contact. Thus, while a particle may be above its threshold of motion due to the shear applied by the local fluid flow, it can be held in place because of neighboring particles which are below their threshold of motion. Thus, collective motion can occur when particles with higher than average erosion thresholds, that are located downstream, are dislodged.

We next obtain the fluid velocity within the system assuming the Poisson equation $\nabla \cdot (\kappa \nabla P) = 0$, where κ is the local permeability which depends on ϕ, and P is the pore pressure. Then, by performing experiments measuring the pressure gradient across a uniformly filled chamber, we have $\kappa(\phi) = 0.285(1-2.14\phi)$ mm^2 for $0 \leq \phi \leq 0.45$. Numerically solving the Poisson equation on a square grid using the method of relaxation, we obtain the fluid velocity $\mathbf{v}_f = -(\kappa/\nu)\nabla P$. A test comparison of the fluid flow obtained numerically and those observed in experiments is found to be in good agreement [24]. Figures 2(f)–2(j) show the local magnitude of the fluid velocity $v_f = |\mathbf{v}_f|$ obtained numerically along with the streamlines of the fluid flow. A contour line corresponding to half the maximum ϕ indicates the relative locations of the high and low porosity regions. The shape of the interface leads to convergence of the fluid streamlines to where the interface is concave before spreading out. Further, v_f is greatest inside the channels where the medium has eroded and where the interface concavity has increased which leads to further increase in fluid flow to that region. From the velocity maps, we also infer that the eroded particles move further before they redeposit as J_f is increased. The redeposition occurs because v_f decreases as the fluid spreads out as it emerges into the higher porosity region [see streamlines in Figs. 2(f)–2(h)]. Because the amount of sediments that a fluid can carry is related to the velocity of the fluid flow [30], this causes the particles to redeposit, as evidenced by the fan which develops in the later stages shown in Figs. 2(c)–2(e).

The mean force acting on a stationary particle due to the viscous drag is linearly proportional to v_f, ν, and d. Because the fluid viscosity and the particles are not varied

in our experiments, we only examine the functional dependence of the fluid velocity on stress. Further, one can expect the effective stress due to the drag to be proportional to ϕ. While a detailed form of the stress will depend on the geometry of the packing, it is expected that the stress goes to zero when $\phi \to 0$. For these reasons, we use the product $v_f\phi$ to gauge the hydrodynamic stress acting on the medium. From the corresponding PDFs shown in Figs. 2(k)–2(o), it can be noted that $v_f\phi \lesssim 8$ mm s^{-1} indicated by the vertical dashed line in each case, while v_f itself can range up to 30 mm s^{-1}. Thus, in regions where $\phi \sim 0.43$, $v \lesssim 18.6$ mm^{-1}, which is at the lower end of the J_c needed to dislodge a single particle in the system. Hence, we conclude that the spatial distribution of the porosity organizes itself such that the system remains near the threshold needed to erode the most weakly held particles in the system once the condition for erosion is reached. For this reason, J_f needs to be ramped up to further evolve the porosity of the system.

To further investigate the effect of porosity inhomogeneity on erosion, we performed experiments with various curvatures of the initial interface. Figures 4(a)–4(c) show
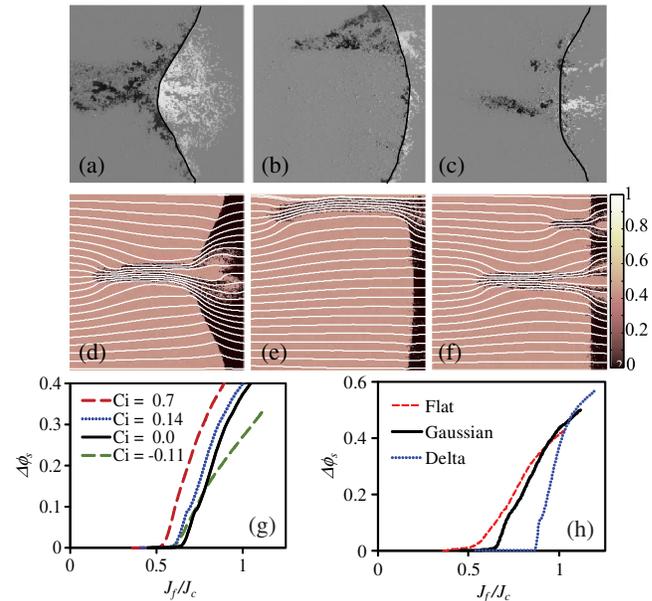

FIG. 4. Difference images indicating regions where erosion (black) and deposition (white) have occurred in experiments with (a) $C_i = 0.7$, $J_f/J_c = 0.53$, (b) $C_i = -0.24$, $J_f/J_c = 0.83$, and (c) $C_i \approx 0$, $J_f/J_c = 0.83$. The line indicates the location of the initial interface. (d)–(f) Maps of the volume fraction ϕ_s and the streamlines observed in corresponding simulations with idealized interfaces (d) $C_i = 0.7$, $J_f/J_c = 0.59$, (e) $C_i = -0.11$, $J_f/J_c = 0.66$, and (f) $C_i = 0$, $J_f/J_c = 0.67$. (g) $\Delta\phi_s$ in the simulations is observed to decrease with magnitude of C_i. (h) The distribution of thresholds used affects the onset of erosion, but its overall progress remains similar well above onset.

snapshots of experiments performed with various idealized interfaces. To highlight the regions where erosion and deposition have occurred, we show the differences of images for a given flow rate with an image taken before the flow was applied. The shape of the initial interface is characterized by the curvature C_i given by the ratio of the system width W and the radius of curvature of the interface at the center. We find that while a channel grows in the middle when the interface is concave, the channel grows typically at the side in case of a convex interface. Further, more channels typically start to grow when the interface is flatter under otherwise similar conditions.

Based on these observations, we have developed a statistical model to simulate and understand the main features needed to capture the flow-dependent evolution of an erodible medium. We use a square grid to partition the system and initialize the sites with a volume fraction ϕ_s drawn randomly between 0.40 and 0.45 to represent areas where particles are present, and zero otherwise. Each lattice site is assigned an erosion threshold e_n with a distribution similar to that measured in the experiments [24] to capture the effect of particle size and sphericity variation. The fluid velocity is then computed by numerically solving the Poisson equation with an imposed flux which is ramped up linearly as in the experiments. Then, erosion is assumed to occur only at lattice sites which border empty sites and if the fluid velocity is found to exceed e_n at that location due to the force exerted by the fluid flowing through that site. Further, particles at a particular site are also assumed to erode if the flow in a neighboring site exceeds a critical value e_t to simulate the effect of tangential shear in dislodging particles. The eroded material is assumed to be transported by the fluid flow with a velocity which is half the local fluid velocity based on the typical motion of particles observed in the experiments. We also assume that the moving particles experience a 5% lateral migration at random toward the direction with lower v_f to simulate observation that the particles are pushed sideways out of the way by the moving fluid. The eroded material is assumed to be deposited if the fluid velocity falls below e_n at that lattice site to capture observations. Further, the particles are assumed to be deposited if their motion is obstructed by the presence of sites with $\phi_s > 0.40$ along their trajectory.

Figures 4(d)–4(f) show the erosion patterns obtained using the simulations corresponding to experiments with similar curvatures as in Figs. 4(a)–4(c). In each simulation, we have assumed that the average $e_n = J_c$ and $e_t = 2.5J_c$, where J_c is chosen to have a Gaussian distribution with the mean and standard deviation similar to that measured in the experiments. We observe similar overall development of porosity with channels forming where fluid can be expected to converge given the overall curvature of the interface. In all cases, one observes that channelization is well progressed even though $J_f < J_c$. As we show next using the simulations, this occurs because of not only the

convergence of flow but also the distribution of threshold for erosion of individual particles.

The effect of the curvature on J_c needed to erode a channel is examined by plotting the eroded volume fraction of the particles in the simulations $\Delta\phi_s$ in Fig. 4(g) for $C_i \geq 0$. It can be noted that erosion starts at a lower J_f in the case of higher C_i. This is consistent with the fact that a greater fraction of fluid converges to a region with higher curvature as evident from the streamlines of the flow in Fig. 4. We also plot in Fig. 4(g) $\Delta\phi_s$ in the case of the convex interface shown in Fig. 4(e). Here, erosion starts at a lower J_f/J_c compared to a flat interface and comparable to the concave case with similar magnitude of curvature. One can understand both these observations in the context of the fluid flow resulting from such an initial interface. Because of the convex interface, the flow is distributed to the sides leading the channels to develop near the side of the system at lower threshold compared to a flat interface. Because of the presence of the side boundaries, less flow converges to the channel that forms leading it to grow less slowly compared to when the channel is formed at the center. Thus, the overall flow geometry and boundary conditions in addition to the interface curvature have to also be taken into account to fully understanding the location and growth of the channels.

The plots of eroded ϕ also show that channels develop at $J_f/J_c < 1$ even in the case of $C_i \approx 0$. To understand this lower onset, even in the case of $C_i \approx 0$, we plot $\Delta\phi_s$ in Fig. 4(h) observed in the simulations using forms of the distributions for J_f other than the Gaussian distribution used to model the observed fluctuations in the threshold. In particular, if e_n is taken to be constant and equal to J_c, i.e., a delta function, we find that erosion commences for J_f/J_c closer to 1. One observes that J_f/J_c still remains somewhat lower than 1 because of the small fluctuations in ϕ_s within the system which leads to local variation in v_f. If, on the other hand, the fluctuations in e_n are increased in the simulations by assuming a flat distribution between $J_f - \sigma_c$ and $J_f + \sigma_c$, we find that erosion commences, comparatively, at slightly lower J_f/J_c. Thus, we conclude from the simulations that the particles which dislodge at lower threshold of fluid flow, i.e., the weakest, lead to greater porosity in that region. The resulting higher flow causes the particles that have greater threshold of erosion to then also erode. This feedback is observed to lead to robust growth of channels for J_f/J_c well below 1. Nonetheless, the detailed nature of the distribution is not observed to affect the overall progress of erosion with similar growth of $\Delta\phi_s$ for large enough J_f/J_c as in Fig. 4(h).

In summary, we have demonstrated that flow through a thin porous medium results in the development of channels which grow upstream due to a convergence of fluid flow similar to those observed in curvature driven seepage erosion systems. Further, a multiscale model which uses

a statistical physics approach has been observed to capture the overall evolution of porosity in the experiments.

*Corresponding author.
akudrolli@clarku.edu

[1] G. Daccord and R. Lenormand, Nature (London) **325**, 41 (1987).

[2] P. Dietrich, *Flow and Transport in Fractured Porous Media* (Springer, New York, 2005).

[3] K. Khilar and H. S. Fogler, *Migration of Fines in Porous Media* (Kluwer, Dordrecht, 1998).

[4] *Internal Erosion of Dams and Their Foundations: Selected and Reviewed Papers from the Workshop on Internal Erosion and Piping of Dams and Their Foundations, Aussois, France, 2527 April 2005*, edited by R. Fell and J. J. Fry (Taylor & Francis, London, 2007).

[5] B. Cailly, P. Le Thiez, P. Egermann, A. Audibert, S. Vidal-Gilbert, and X. Longaygue, Oil Gas Sci. Technol. Rev. IFP **60**, 517 (2005).

[6] P. Gouze and L. Luquot, J. Contam. Hydrol. **120–121**, 45 (2011).

[7] T. S. Lo and J. Koplik, Phys. Fluids **24**, 053303 (2012).

[8] M. Weingarten, S. Ge, J. W. Godt, B. A. Bekins, and J. L. Rubinstein, Science **348**, 1336 (2015).

[9] C. G. Groves and A. D. Howard, Water Resour. Res. **31**, 19 (1995).

[10] P. Szymczak and A. J. C. Ladd, Geophys. Res. Lett. **38**, L07403 (2011).

[11] Samuel A. Ocko and L. Mahadevan, Phys. Rev. Lett. **114**, 134501 (2015).

[12] T. Dunne, Prog. Phys. Geogr. **4**, 211 (1980).

[13] A. D. Howard and C. F. McLane, Water Resour. Res. **24**, 1659 (1988).

[14] N. Schorghofer, B. Jensen, A. Kudrolli, and D. H. Rothman, J. Fluid Mech. **503**, 357 (2004).

[15] D. M. Abrams, A. E. Lobkovsky, A. P. Petroff, K. M. Straub, B. McElroy, D. C. Mohrig, A. Kudrolli, and D. H. Rothman, Nat. Geosci. **2**, 193 (2009).

[16] P. G. Saffman and G. I. Taylor, Proc. R. Soc. A **245**, 312 (1958).

[17] O. Johnsen, R. Toussaint, K. J. Maloy, and E. G. Flekkoy, Phys. Rev. E **74**, 011301 (2006).

[18] X. Cheng, L. Xu, A. Patterson, H. M. Jaeger, and S. R. Nagel, Nat. Phys. **4**, 234 (2008).

[19] R. Holtzman, M. L. Szulczewski, and R. Juanes, Phys. Rev. Lett. **108**, 264504 (2012).

[20] B. Sandnes, E. G. Flekkoy, H. A. Knudsen, K. J. Maloy, and H. See, Nat. Commun. **2**, 288 (2011).

[21] A. Mahadevan, A. V. Orpe, A. Kudrolli, and L. Mahadevan, Europhys. Lett. **98**, 58003 (2012).

[22] O. Singurindy and B. Berkowitz, Water Resour. Res. **39**, 1143 (2003).

[23] O. Zvikelsky and N. Weisbrod, Water Resour. Res. **42**, W12S08 (2006).

[24] See the Supplemental Material at http://link.aps.org/supplemental/10.1103/PhysRevLett.117.028001 for a video of the system evolving as the flow is increased as in Fig. 2, characterization of initial volume fluctuations, and tests of the flow simulations.

[25] A. Hong, M. Tao, and A. Kudrolli, Phys. Fluids **27**, 013301 (2015).

[26] J. A. Eriksen, B. Marks, B. Sandnes, and R. Toussaint, Phys. Rev. E **91**, 052204 (2015).

[27] M. Berhanu, A. Petroff, O. Devauchelle, A. Kudrolli, and D. H. Rothman, Phys. Rev. E **86**, 041304 (2012).

[28] H. Seybold, J. S. Andrade, Jr., and H. J. Herrmann, Proc. Natl. Acad. Sci. U.S.A. **104**, 16804 (2007).

[29] H. M. Jaeger, C.-H. Liu, and S. R. Nagel, Phys. Rev. Lett. **62**, 40 (1989).

[30] G. P. Williams, J. Hydrol. (Amst.) **111**, 89 (1989).